RESEARCH PAPER

Horizontally networked carbon nanotubes grown on Au–Fe catalyst nanoparticles

Muhammad Aniq Shazni Mohammad Haniff · Hing Wah Lee · Daniel C. S. Bien · Ishak Abd. Azid

Abstract Horizontally networked carbon nanotubes grown on Au–Fe catalyst nanoparticles were achieved through the decomposition of acetylene by plasma-enhanced chemical vapor deposition (PECVD) method. It has been ascertained that conditions governing the formation of the bilayer Au–Fe catalyst nanoparticles dictate the resultant growth of the nanotubes. From the FESEM and AFM studies, the average nanoparticle size was found to increase in the range of 13.3–87.0 nm as the catalyst film thickness increases. A net-like structure of multi-walled carbon nanotubes network with the remains of Au clusters on the substrate was observed for the thicker catalyst, suggesting the absence of nanotube growth on these Au clusters due to catalyst deactivation. Possible mechanisms of nanotube growth dependent catalyst formation are discussed in the paper, which explain the role of Au film in the growth stage. The influence of ammonia to acetylene gas ratios on the sheet resistance, sheet concentration, average sheet Hall coefficient, and magnetoresistance of the grown nanotubes was discussed.

Keywords Carbon nanotubes · Catalyst · Chemical vapor deposition · Au–Fe · Hall effect · Composite nanomaterials · Thin layers

M. A. S. M. Haniff (✉) · H. W. Lee · D. C. S. Bien
Nanoelectronics Lab, MIMOS Berhad, Technology Park
Malaysia, 57000 Kuala Lumpur, Malaysia
e-mail: aniq.haniff@mimos.my

H. W. Lee
e-mail: hingwah.lee@mimos.my

D. C. S. Bien
e-mail: daniel.bien@mimos.my

M. A. S. M. Haniff · I. A. Azid
School of Mechanical Engineering, USM Engineering
Campus, Universiti Sains Malaysia, 14300 Nibong Tebal,
Pulau Pinang, Malaysia
e-mail: ishak.abdulazid@unikl.edu.my

I. A. Azid
Mechanical Section, Universiti Kuala Lumpur Malaysian
Spanish Institute, 09000 Kulim Hi-TechPark, Kedah,
Malaysia

Introduction

Carbon nanotubes (CNTs) have been extensively studied for large-scale integration of nanoelectronics structure since their discovery in 1991 (Iijima 1991). Due to their outstanding electronic, mechanical, and electromechanical properties, they are designated as one of the most desirable materials for numerous potential applications such as field emitters (Yin et al. 2008), atomic force microscopy tips (Yenilmez et al. 2002), transistors (Choi et al. 2001), and supercapacitors (Kim et al. 2012). CNTs can mainly be classified into two which are single-walled carbon nanotubes (SWCNTs) and multi-walled carbon nanotubes (MWCNTs). It has been commonly perceived that

the MWCNTs grown via chemical vapor deposition (CVD) are strongly dependent on the formation of catalyst, supportive layer type, and ratio of feed gases and temperature. Kukovecs et al. (2000) and Lee et al. (2002) have done extensive study in terms of the catalytic activity of typical transition metal catalyst such as Co, Fe, and Ni in the formation of nanotubes. It was demonstrated that the catalyst formation would have their optimum catalytic activity at different initial film thickness, substrate type, annealing temperature, and the duration of applied plasma (Haniff et al. 2014; Wang et al. 2007; Nessim et al. 2008).

It is known that a low temperature synthesis of MWCNTs by CVD has higher structural defects such as vacancies, dislocations, dangling bonds, and rehybridization which results in a modification of their electronic properties (Charlier 2002). In order to reduce these defects, a high growth temperature is required to enhance the structural orders so that well-graphitized straight nanotubes could be obtained (Chhowalla et al. 2001). Behler et al. (2006) and Zhao et al. (2012) demonstrated the role of thermal treatment to further eliminate the structural defects in tube walls, but can only succeed at elevated temperatures above 1,800 °C. Furthermore, it was reported that nanotube quality can be enhanced by utilizing appropriate ratio of acetylene to ammonia gas in the presence of plasma during the growth process to achieve amorphous carbon-free growth (Teo et al. 2001). However, these findings are catalyst-specific, where CNTs are grown on single metal catalyst nanoparticles and yet to be clarified for bilayer type metal catalyst nanoparticles.

Multilayer metal catalysts such as Fe–Ni, Co–Ni, Fe–Mo, and Zr–Ni have been utilized to improve the yield and crystallinity of nanotubes due to their catalytic synergies (Fazle Kibria et al. 2002; Sun et al. 1999; Christen et al. 2004; Kumar et al. 2013). In this case, the use of diffusion barrier layers such as TiN or Al_2O_3 is necessary in order to optimize the catalyst surface and subsequently increase the rate of yield (García-Céspedes et al. 2009; Liu et al. 2008). Additionally, the plasma-pretreated catalyst also shows its capability to nucleate and produce highly dense nanotubes formation by enhancing the catalyst activity and stability onto the substrate (Esconjauregui et al. 2011). Horizontally aligned nanotubes with low network density can also be synthesized using CVD. To date, very few studies have been carried out to understand its growth mechanism. Reina et al. (2007) reported the use of catalyst pretreatment and longer growth duration to produce long and horizontally aligned nanotubes. Meanwhile, Zhang et al. (2013) demonstrated the growth of aligned MWCNTs based on the influence of tip-growth mechanism which is catalyzed by small-sized nanoparticles. This finding shows that both size and catalytic life time of the nanoparticles is the most probable reason leading to this growth formation.

Recently, horizontally oriented MWCNTs with high uniformity and low network density are more favorable in enhancing electrical transport between the electrical contacts for integration in nanoelectronics devices (Tawfick et al. 2009). However, there are still a lot of challenges in being able to control its thinner density without losing its excellent uniformity, structural, and electrical properties. In this paper, a feasibility study of horizontally networked MWCNTs selectively grown on Au–Fe catalyst nanoparticles by PECVD is presented. Results from detailed characterization of catalyst formation on supportive TiN layer under plasma treatment when varying the initial catalyst thickness for earlier nucleation stage of MWCNTs are presented. Instead of the supported Fe catalyst nanoparticles, we expect the introduction of Au layer as passive catalyst leads to better growth formation of horizontally networked MWCNTs. In addition, the effect of ammonia and acetylene gas ratio to the resultant MWCNTs in term of morphological evolution, structural quality, and electrical characterization is discussed.

Experimental

MWCNTs were grown onto supported Au–Fe catalyst nanoparticles by PECVD in an Oxford Instruments Nanofab-700 system at ambient pressure. A catalytic thin Au–Fe films (4–10 nm) with a diffusion barrier of TiN (10 nm) were deposited on a thermally oxidized Si (100) substrate through radio-frequency magnetron sputtering at a base chamber pressure of $\sim 10^{-3}$ mbar and temperature of 42 °C. The Au and Fe thin films were sputtered at 1:1 thickness ratio, in which these two metal thin films have a similar thickness. For example, a total catalyst thickness of 10 nm, a 5 nm Au thin film was sputtered on top of a 5 nm Fe thin film. Prior to CNT growth, the as-sputtered films were

annealed in vacuum at 700 °C for 10 min in hydrogen (100 sccm), with an applied plasma power of 200 W. This short plasma pretreatment step resulted in a formation of small nanoparticles. By maintaining a temperature of 700 °C, the nanotubes were subsequently grown on the seeds in the same furnace chamber with 50 sccm of acetylene (C_2H_2) at a pressure of 1,000 mTorr for 30 min. Further nanotubes growth process on a 10 nm pre-treated catalyst was performed in ammonia (NH_3)/acetylene (C_2H_2) environment with various gas ratios of 0.5:1, 1:1, 2:1, and 4:1. The C_2H_2 flow rate was fixed at 50 sccm.

Both the nucleated nanoparticles and the as-grown nanotubes were characterized using a field emission scanning electron microscopy system (JEOL JSM-7500F). The surface morphology of the nucleated Au–Fe catalyst nanoparticles was examined in an atomic force microscopy system (NT-MDT NTEGRA Spectra) under semi-contact mode to evaluate the distribution of the nanoparticles size and height, and also RMS-roughness of the catalyst surface. The individual nanotube structure was characterized with a high-resolution transmission electron microscopy (HRTEM) system, operating at 200 kV accelerating voltage. In order to characterize the quality of the as-grown nanotubes, the Raman spectra of the nanotubes were obtained using a Raman spectroscopy system (NT-MDT NTEGRA Spectra). A 473 nm air-cooled laser was focused on a diffraction limited resolution of 250 nm, and the acquisition time was accumulated up to 5 min. For the electrical properties, the sheet resistance, sheet concentration, average Hall sheet coefficient, and magnetoresistance were measured with a Hall effect measurement system (Ecopia-HMS5300) based on the van der Pauw method at room temperature with an excitation current of 1 mA and an applied magnetic field (B) of 0.55 T.

Results and discussion

Figure 1 shows the morphology distribution of Au–Fe nanoparticles formed with initial catalyst film thickness from 4 nm to 10 nm after annealing under plasma pretreatment for 10 min. The as-deposited Au–Fe film is known to break up into small nanoparticles in a formation of seeding layers at elevated temperature due to surface tension and compressive stress between the Au–Fe film and the TiN layer/oxidized Si (100)

substrate. These seeding layers can act as nucleation sites for subsequent catalytic nanotube growth. It was observed that the presence of hydrogen in the plasma pretreatment step not only restructures and enables agglomeration of the Au–Fe thin films, but also leads to catalyst coarsening to form better catalyst formation.

From the SEM results in Fig. 1a–d, the agglomeration of Au and Fe thin films differs slightly due to the variation of lattice mismatch in thermal expansion coefficient with minimal interaction between these catalysts. It was observed that the size distribution of the Au–Fe nanoparticles is dependent on the initial catalyst thickness based on the fact that the nanoparticles size increases with thicker initial catalyst film. Meanwhile, the nanoparticle density decreases by approximately 70 % when increasing the initial catalyst film thickness from 4 nm to 10 nm. At low catalyst film thickness of 4 nm (see Fig. 1a), the film was completely disintegrated into an isolated formation of mostly circular nanoparticles due to effect of least particle coalescence during agglomeration. Through short plasma pretreatment, a thinner catalyst film was found to rapidly agglomerates, thus forming isolated nanoparticles of small diameters with minimal inter-particle distance. Through the SEM images, it is difficult to differentiate the elements of pure Au and Fe particles because of the homogeneous particle size. In this case, there is a possibility of inter-diffusion occurring between the Au and Fe atoms. In contrast, with thicker catalyst film of 8 nm (see Fig. 1c), the films start to coalesce into a formation of elongated Au clusters with small-sized Fe nanoparticles. Meanwhile, if the catalyst film is increased to 10 nm (see Fig. 1d), the Au film agglomerates into a clustered network of islands on the surface of the small-sized Fe nanoparticles which has larger void nucleation domain as a result of grain boundary grooving. However, there is still a possibility of inter-diffusion of Au atoms and Fe to form alloying nanostructures especially at the boundary of the large Au islands.

The nanoparticles height and roughness have been evaluated based on the AFM images shown in Fig. 1e–h. The nanoparticles height distribution increases by 2–10 % as compared to its initial catalyst thickness. For the 4 nm thick catalyst film, a much more uniform distribution of nanoparticles was achieved as a result of small grains formation with an average nanoparticle
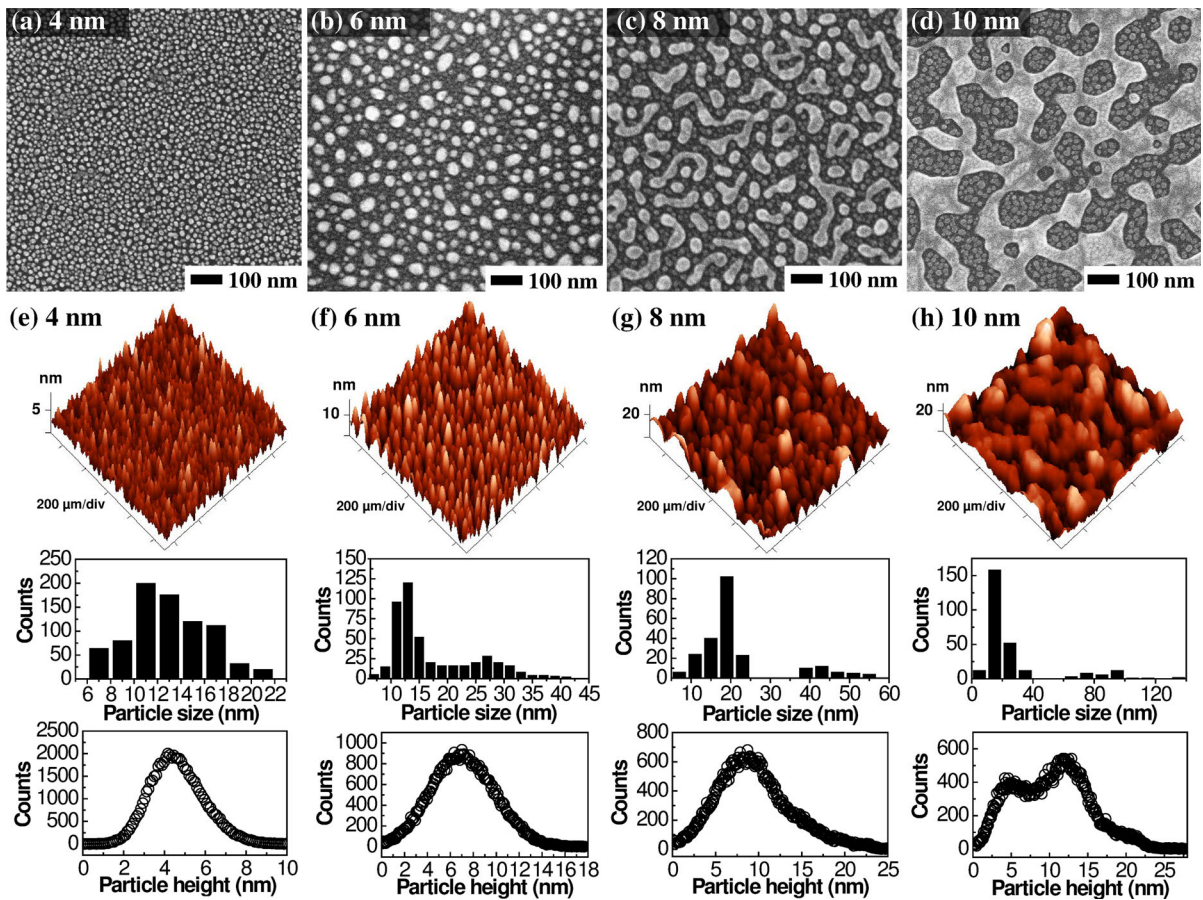
Fig. 1 The morphology of catalyst formation after 10 min plasma treatment at 700 °C: **a–d** SEM images of the nucleated Au–Fe catalyst nanoparticles at different initial catalyst film thickness and **e–f** their corresponding AFM images. The *insets* show the size and height distribution of nanoparticles

Table 1 Characteristics of catalyst nanoparticles formation at different initial catalyst thickness and their corresponding nanotube growth

Initial catalyst thickness (nm)	Average particle size (nm)	Average particle height (nm)	Roughness -RMS (nm)	Particle density ($\times 10^{11}$/ cm^2)	Carbon-shell/ nanotube diameter (nm)	Nanotube density ($\times 10^{11}$/ cm^2)
4	13.3 ± 3.5	4.1	1.21	3.12	23.7 ± 3.2	–
6	13.5 ± 2.5 (Fe) 27.7 ± 4.9 (Au)	6.6	2.79	1.84	40.1 ± 13.9	–
8	17.4 ± 4.3 (Fe) 45.4 ± 9.2 (Au)	8.8	4.38	1.06	7.1 ± 1.2	1.05
10	18.7 ± 5.7 (Fe) 87.0 ± 17.1 (Au)	5.5 (Fe) 11.8 (Au)	4.81	0.91	8.8 ± 1.2	2.23

The initial Au–Fe thickness was fixed at 1:1 ratio

height of 4.1 nm. Meanwhile, the non-uniform distribution of nanoparticles, which contains a mixture of smaller and larger grain formation, was observed for 6, 8, and 10 nm thick catalyst films with an average nanoparticle height of 6.6, 8.8, and 10.2 nm, respectively. The measured nanoparticles surface roughness
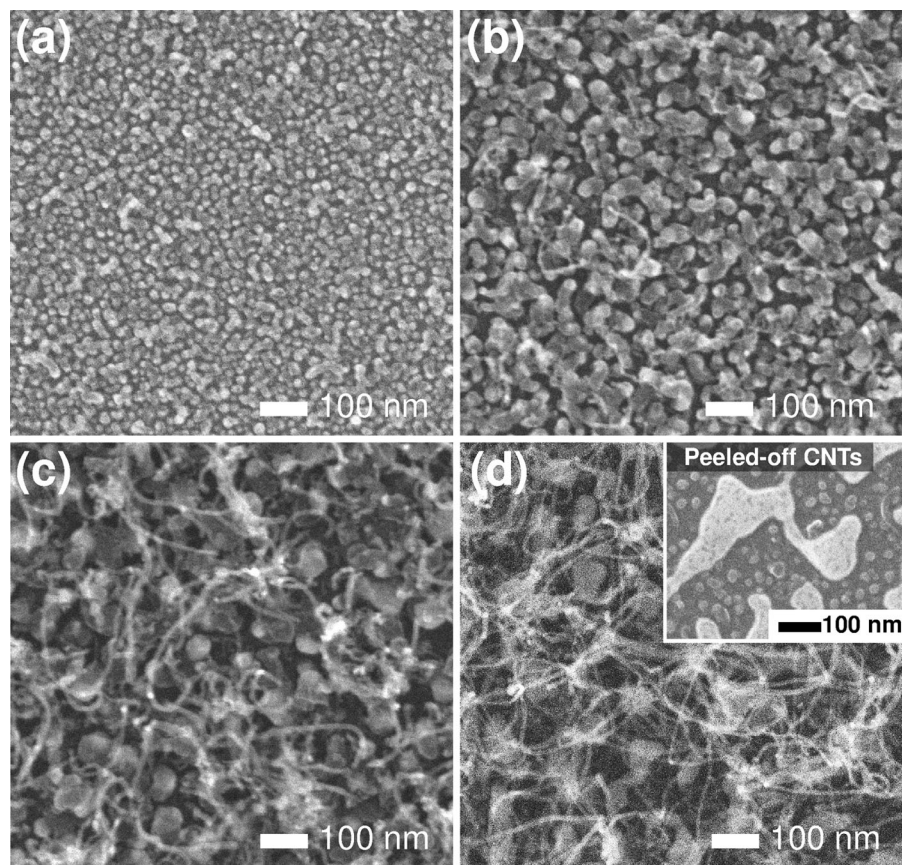
Fig. 2 FESEM images of MWCNTs grown on different initial catalyst film thickness by the use of acetylene as precursor: **a** 4 nm, **b** 6 nm, **c** 8 nm and **d** 10 nm. The *inset* shows the SEM images of the peeled-off nanotubes network

for the 10 nm thick catalyst film is approximately four times higher than that of the 4 nm thick catalyst film (see Table 1). The significant increase in surface roughness is mainly attributed to the broader nanoparticles size distribution.

Figure 2a–d shows the FESEM images of nanotubes grown directly by acetylene decomposition onto the catalyst with thicknesses of 4 to 10 nm. It was observed that there is almost no nanotube growth for both 4 and 6 nm thick catalyst film. Instead, a formation of carbon-coated catalyst nanoparticles could be observed with a diameter of 23.7 ± 3.2 nm and 40.1 ± 13.9 nm for the 4 and 6 nm thick catalyst films, respectively. The size of carbon-coated catalyst nanoparticles increases by approximately 80–130 % as compared to their nanoparticles size before the growth process, thus indicating the presence of carbon formation on the catalyst surface. Meanwhile, a

formation of horizontally networked nanotubes and the remains of Au clusters on the substrate were observed for the thicker catalyst film of more than 6 nm, indicating the absence of nanotube growth on these Au clusters. In this case, the coalescence of Au clusters forms a passivation layer to suppress the nanotube growth. Results also show that the densest nanotube formation was grown on the 10 nm thick catalyst film, with an outer diameter of 8.8 ± 1.2 nm and density of $2.23 \times 10^{11}/cm^2$. The measured outer diameter distribution and density of nanotube is lower compared to that of catalyst size. This could be attributed to the restriction of nanotube growth directly on the catalyst due to strong interaction between Fe particles and the supportive TiN layer. It is expected that this interaction resulted in a predominant base or root growth mechanism, in which the majority of Fe particles were strongly attached on the substrate

Fig. 3 Schematic representation of growth mechanism for horizontally networked MWCNTs grown on 10 nm thick Au–Fe catalyst nanoparticles by decomposition of acetylene
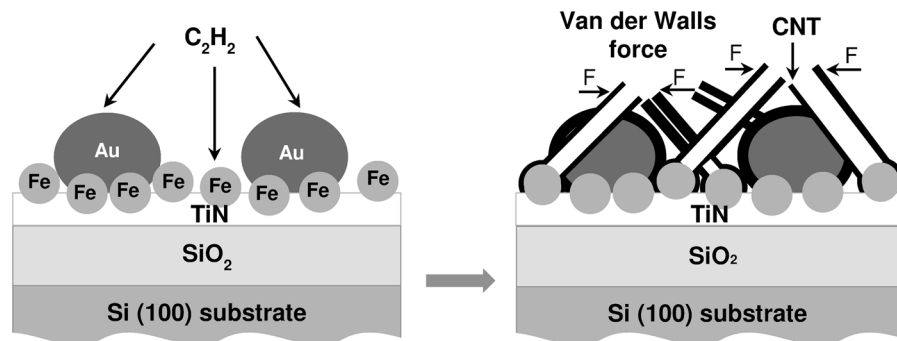
after peeling-off nanotubes as shown in the inset of Fig. 2d. However, there is still a minor possibility that a small amount of Fe particles being removed due to formation of MWCNTs through a tip-growth mechanism. The characteristics of catalyst formation at different initial thickness and the resultant nanotube growth are summarized in Table 1.

For the nucleated catalyst at film thickness lower than 6 nm, it is expected that the Au and Fe nanoparticles or their alloying nanoparticles with narrower size distribution became inactive and more easily poisoned by the interface of amorphous carbon. The precipitation of carbon feedstock with larger amount of amorphous carbon on these catalyst surfaces possibly occurs at a greater rate during the nucleation phase. At the early stage of nanotube growth, it is probable that the amorphous carbon might be more readily deposited on the surface of these nanoparticles, thus preventing the nanotube growth. In addition, the formation of Au nanoparticles on the surface of Fe nanoparticles could also prevent the carbon nanotubes from growing at a higher rate. In contrast, for a 10 nm thick catalyst film, the nanotubes were grown on the nucleated Fe nanoparticles, which were formed in the void nucleation domains. The resultant domains provide a better interaction between Fe nanoparticles and carbon feedstock which leads to higher nanotube density. During the nanotube growth, the presence of continuous Au layer on the surface of the Fe nanoparticles not only prevents a high diffusion rate of carbon feed-stocks onto the catalyst surface, but also may initiate the nanotube growth directly towards horizontal direction, parallel to the substrate. The ends of the nanotubes were found to be cross-

linked among the neighboring nanotubes in a form of net-like structure (see Fig. 2d) due to attractive forces of intertube van der Waals, thereby resulting in a better growth formation of horizontally networked carbon nanotubes. The proposed growth mechanism of horizontally networked MWCNTs grown on Au–Fe catalyst nanoparticles is shown in Fig. 3.

The interior and wall structures of the nanotubes grown on the Au–Fe catalyst nanoparticles are determined using HRTEM. Figure 4a–b and Fig. 4c show a cross-sectional view of the resultant nanotube, consists of thinner (without ammonia) and thicker tube-walls (with ammonia), respectively. For thinner tube-walls, the TEM image shows that the nanotube is of multi-walled type with hollow central feature. The lattice fringes on each side of the tube indicate individual cylindrical graphitic layers with approximately 7–8 walls of graphitized carbon. The graphitic layer was measured to be approximately 0.34 nm, which is in good agreement with the common graphite spacing (Amelinckx et al. 1994). Meanwhile, a bamboo-like structure with approximately 16–20 walls of graphitized carbon was observed for the thicker tube-walls. This particular tube consists of hollow compartments with 4–5 graphite walls separated with a distance of approximately 25 nm. The graphitic walls running across the diameter of the nanotube indicates that the structural defects formed were due to twisting of the nanotube structure. Formation of amorphous carbon at the outer walls of nanotubes can be seen from the images in Fig. 4a–b. In addition, the structure of carbon-coated Au clusters is shown in Fig. 4d–e, where the absence of the nanotube formation on the Au clusters was observed, but a
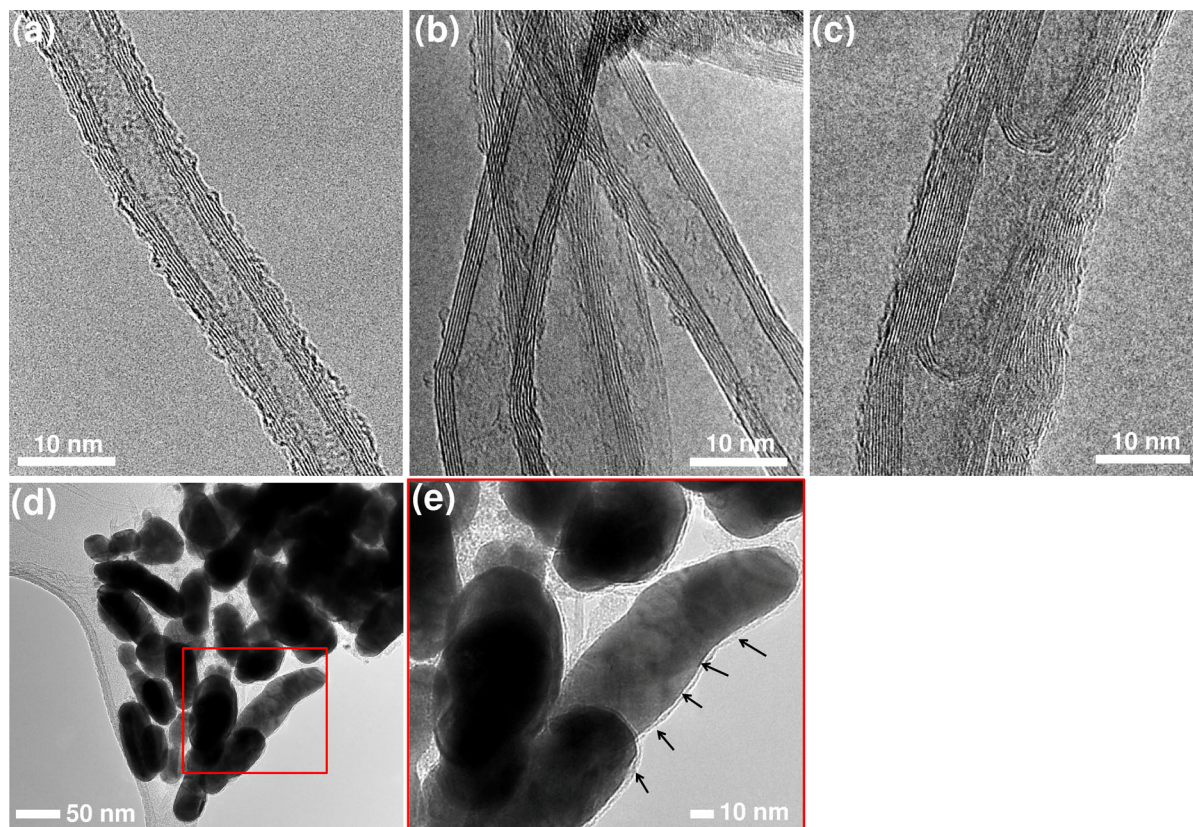
Fig. 4 HRTEM images of as-grown MWCNTs over supported Au–Fe catalyst nanoparticles: **a–b** central hollow structure for thinner tube-walls (C$_2$H$_2$ only), **c** bamboo-like structure for thicker tube-walls (NH$_3$/C$_2$H$_2$ = 200 sccm/50 sccm), **d** amorphous carbon-coated Au clusters and **e** close-up view. The *arrows* indicate the presence of amorphous carbon layer on the surface of Au clusters
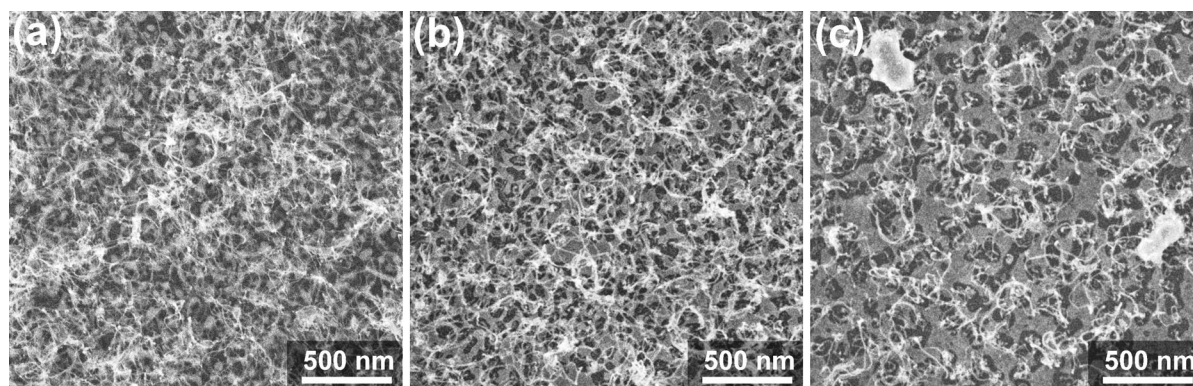

Fig. 5 FESEM images of MWCNTs grown on initial 10 nm thick Au–Fe catalyst nanoparticles at different NH$_3$/C$_2$H$_2$ gas ratios: **a** 0, **b** 2, and **c** 4. The flow rate of C$_2$H$_2$ was fixed at 50 sccm

2.5 nm thick amorphous carbon was formed on the clusters surface during the prolonged nanotube growth.

The influence of NH$_3$/C$_2$H$_2$ gas ratios on the nanotube growth over Au–Fe catalyst nanoparticles is shown in Fig. 5. It should be noted that the

Table 2 Characteristics of MWCNTs and Raman spectra at different NH_3/C_2H_2 gas ratios

NH_3/C_2H_2 gas ratios, r	Outer diameter of nanotube (nm)	I_D/I_G ratio
0	8.8 ± 1.2	0.883
0.5	9.7 ± 1.0	0.875
1	10.5 ± 1.3	0.868
2	11.4 ± 1.4	0.847
4	14.0 ± 1.2	0.824

Fig. 6 Raman spectra of MWCNTs grown on initial 10 nm thick Au–Fe catalyst nanoparticles at different NH_3/C_2H_2 gas ratios. The weak peak of the Raman mode with a feature marked of '*' at 2,330 cm^{-1} arises from ambient N_2 (molecular) gas in the air surrounding the sample

nanotubes are characteristically different at varying gas ratios, in which the yield of nanotube decreases with the increase of gas ratios. The results indicate that the aggregation of nanotubes was formed with gas ratios of less than two. Conversely, if the gas ratios are increased from 0 (without NH_3) to 4, the outer nanotube diameter increases by approximately 60 %, from 8.8 ± 1.2 nm to 14.0 ± 1.2 nm (Table 2). In the NH_3/C_2H_2 environment, there is a restriction of carbon atoms precipitation onto Fe nanoparticles. When the gas ratio of ammonia to acetylene was greater, the number of nanotubes formed was found to decrease. It is expected that the possibility of acetylene decomposition onto Fe surface occurred at a much lower rate due to greater ammonia concentration, thereby resulting in low-density nanotube formation. Additionally, the observed coalescence of large-sized Au clusters into a continuous film appears at higher gas ratios also results in low-density nanotube formation.

Figure 6 shows the Raman spectra of MWCNTs grown on supported Au–Fe catalyst nanoparticles deposited on TiN/SiO_2 substrate at different NH_3/C_2H_2 gas ratios. From the results strong peaks were observed at approximately 1,365 and 1,588 cm^{-1}, corresponding to D and G-band, respectively, with a 2D-band peak at approximately 2,700 cm^{-1}. The first- and second-order Si peaks are also seen at 520 and 935 cm^{-1}, respectively. However, the Raman signals associated with the radial breathing mode (RBM) from the typical MWCNTs is too poor to be observable, thus it is excluded from the results. The D-band is activated by the vibrations of carbon atoms with dangling bonds in plane termination of disordered graphite associated with defects. The G-band represents the ordered graphite corresponding to the stretching mode of sp^2-bonded carbon atoms in a two-dimensional hexagonal lattice. The intensity I_D/I_G ratio can, therefore, be used to monitor the imperfection of
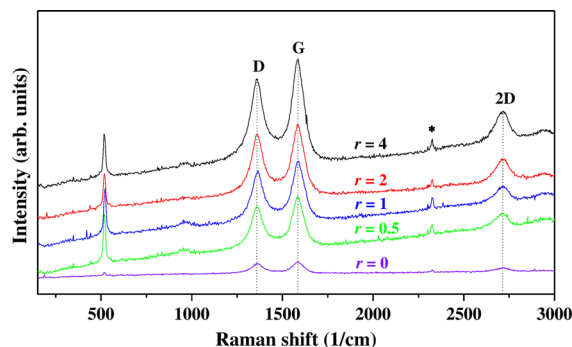
nanotube structure. From Table 2, it was observed that the I_D/I_G ratio decreases at small changes of approximately 7 % with the increase in NH_3/C_2H_2 gas ratio from 0 to 4, indicating an improvement in the nanotube quality: amount of amorphous carbon in MWCNTs decrease. At lower concentration of NH_3, many nanotubes and large-sized Au clusters are possible to be encircled by amorphous carbon that contribute to the D-band because the etching effect of NH_3 becomes less significant, thereby increasing the I_D/I_G ratio. In comparison to the previous studies, it can be ascertained that the nanotubes grown for the present work exhibits lower I_D/I_G ratio than that ($I_D/I_G = 1.24$) of MWCNTs deposited on Co–Ni catalyst at substrate temperature of approximately 600–700 °C (Ryu et al. 2008), and that ($I_D/I_G = 1.18$) of MWCNTs deposited on Au catalyst at substrate temperature of 750 °C (Lee et al. 2005). This shows that the MWCNTs grown on supported Au–Fe catalyst nanoparticles are of higher quality with fewer structural defects.

Electrical characterization based on the van der Pauw technique was performed to evaluate the sheet resistance, sheet concentration, average sheet Hall coefficient, and magnetoresistance (MR) of the resultant MWCNTs. The results of sheet resistance, MR, and sheet concentration as a function of NH_3/C_2H_2 gas ratios are shown in Fig. 7. It was observed that the measured sheet resistance increases by approximately 170 % with the increase of NH_3/C_2H_2 gas ratio from 0 (without NH_3) to 4. The formation of high-density nanotube grown in the absence of ammonia gas shows the lowest sheet resistance of 5.12 kOhms per square
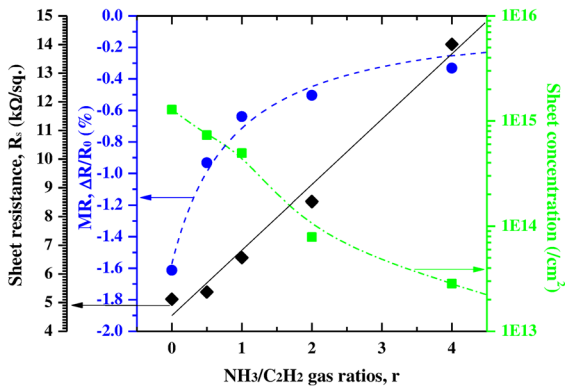
Fig. 7 Sheet resistance, relative magnetoresistance (MR), and sheet concentration as a function of NH_3/C_2H_2 gas ratios

(kΩ/sq.). This notion might be due to the aggregation of nanotubes which leads to increase in channels for conduction. It should be noted as well that the resistance of the nanotubes network is governed mainly by the contact resistance and the tunneling resistance through a gap between adjacent nanotubes or Au clusters. At higher gas ratios, it is expected that the larger end connections of isolated nanotubes network have lower contact area and wider tunneling distance, which consequently lead to the higher resistance value. In contrast, the sheet concentration tends to decrease at higher gas ratio of four. This could be attributed to the presence of larger nanotube diameters, in which the trend is consistent with the findings of Rakitin et al. (2003). In this case, the predominance of hole transport, p-type carriers in the electronic conduction of nanotubes network results in positive average sheet Hall coefficient.

A negative MR was obtained for the resultant growth of MWCNTs as shown in Fig. 7. The relative MR decreases with increasing NH_3/C_2H_2 gas ratios and the largest measured MR was approximately -1.613 % at $T = 293$ K and $B = 0.55$ T from the

formation of MWCNTs/Fe–Au nanoparticles in ammonia-free environment ($r = 0$). Because of the low atomic number of carbon, spin-scattering effects among the nanotubes is negligible, while a large amount of spin-scattering is expected at the interface of nanotubes/Fe nanoparticles or among adjacent Fe nanoparticles. In the mixture of non-magnetic and magnetic nanoparticles, the MR is spin-dependent scattering which is based on granular giant magneto-resistance (GMR) mechanism. For the nanotube growth at $r = 0$, larger number of nanotubes with isolated small-sized Fe nanoparticles is expected to have larger amount of spin-scattering at the interface of nanotube/Fe and adjacent Fe–Au nanoparticles. When the magnetic field of 0.55 T is applied perpendicularly to the surface, the spin at these interfaces enhances the electron transport, allowing the electrons to hop between nanotubes and adjacent Fe–Au nanoparticles, thereby resulting in a larger reduction of in-plane resistance. In contrast, for the nanotube growth at higher gas ratio ($r = 4$), the predominant electrical transport is governed by the continuous Au films. The change in resistance upon applying magnetic field of 0.55 T becomes less significant as a result of minor spin-scattering at the grain boundary, thereby decreasing the MR. The results of electrical characterization of horizontally networked MWCNTs are summarized in Table 3.

Conclusions

In summary, we have demonstrated the synthesis of horizontally networked MWCNTs on Au–Fe catalyst nanoparticles supported TiN by PECVD. The influence of the initial catalyst thickness on the average particle size and density was studied in which results indicated that the difference in the agglomeration of

Table 3 Electrical characterization of MWCNTs based on the van der Pauw method

NH_3/C_2H_2 gas ratios, r	Sheet resistance ($\times 10^3$ Ohm/sq.)	Sheet concentration (/cm²)	Average sheet Hall coefficient (cm²/C)	Magnetoresistance, $\Delta R/R_0$ (%)
0	5.12	1.28×10^{15}	8.60×10^3	-1.613
0.5	5.37	7.33×10^{14}	3.37×10^4	-0.932
1	6.57	4.94×10^{14}	1.11×10^4	-0.639
2	8.53	7.89×10^{13}	9.38×10^4	-0.504
4	14.01	2.84×10^{13}	2.05×10^5	-0.331

Au and Fe nanoparticles is due to the variations in lattice mismatch. In the presence of plasma at high temperature, the catalyst nanoparticles on the substrate tend to agglomerate and coalesce into large ones, thus resulting in increase of average nanoparticles size as the catalyst film thickness increases. By controlling this catalyst nanoparticles formation, the expected nanotube growth could be obtained, in which a formation of densest MWCNTs with a net-like network was observed at thicker catalyst. These MWCNTs tend to follow a predominant base growth mechanism due to strong interaction between the catalyst nanoparticles and the supported TiN layer. We have also demonstrated the influence of the mixture ratios between ammonia and acetylene on the nanotube growth. A significantly larger nanotube diameter was obtained with higher ammonia to acetylene gas ratio. Results from the Raman spectra also show that nanotubes formed through higher gas ratio of 4 with larger diameter exhibited lower I_D/I_G ratio of 0.824, indicating an improvement in the nanotube quality. For the electrical characterization, growing a higher nanotube density may result in some improvement in sheet resistance due to the nanotube aggregation, in which leads to increase in channels for conduction.

References

Amelinckx S, Zhang XB, Bernaerts D, Zhang XF, Ivanov V, Nagy JB (1994) A formation mechanism for catalytically grown helix-shaped graphite nanotubes. Science 265:635–639. doi:10.1126/science.265.5172.635

Behler K, Osswald S, Ye H, Dimovski S, Gogotsi Y (2006) Effect of thermal treatment on the structure of multi-walled carbon nanotubes. J Nanopart Res 8:615–625. doi:10.1007/s11051-006-9113-6

Charlier J-C (2002) Defects in carbon nanotubes. Ac Chem Res 35:1063–1069. doi:10.1021/ar010166k

Chhowalla M, Teo KBK, Ducati C, Rupesinghe NL, Amaratunga GAJ, Ferrari AC, Roy D, Robertson J, Milne WI (2001) Growth process conditions of vertically aligned carbon nanotubes using plasma enhanced chemical vapor deposition. J Appl Phys 90:5308–5316. doi:10.1063/1.1410322

Choi WB, Chu JU, Jeong KS, Bae EJ, Lee J, Kim J (2001) Ultrahigh-density nanotransistors by using selectively grown vertical carbon nanotubes. Appl Phys Lett 79:3696–3698. doi:10.1063/1.1419236

Christen HM, Puretzky AA, Cui H, Belay K, Fleming PH, Geohegan DB, Lowndes DH (2004) Rapid growth of long, vertically aligned carbon nanotubes through efficient catalyst optimization using metal film gradients. Nano Lett 4:1939–1942. doi:10.1021/nl048856f

Esconjauregui S, Bayer BC, Fauquet M, Wirth CT, Yan F, Xie R, Ducati C, Baehtz C, Castellarin-Cudia C, Bhardwaj S, Cepek C, Hofmann S, Robertson J (2011) Use of plasma treatment to grow carbon nanotube forests on TiN substrate. J Appl Phys 109:114312. doi:10.1063/1.3587234

Fazle Kibria AKM, Mo YH, Nahm KS (2002) Synthesis of narrow-diameter carbon nanotubes from acetylene decomposition over an iron-nickel catalyst supported on alumina. Carbon 40:1241–1247. doi:10.1016/S0008-6223(01)00298-6

García-Céspedes J, Álvarez-García J, Zhang X, Hampshire J, Bertran E (2009) Optimal deposition conditions of TiN barrier layers for the growth of vertically aligned carbon nanotubes onto metallic substrate. J Phys D Appl Phys 42:104002. doi:10.1088/0022-3727/42/10/104002

Haniff MASM, Lee HW, Bien DCS, Azid IHA, Lee MW, Embong SS (2014) Formation of Co, Fe and Co-Fe nanoparticles through solid-state dewetting in the presence of hydrogen plasma and their electrical properties. Vacuum 101:371–376. doi:10.1016/j.vacuum.2013.10.015

Iijima S (1991) Helical microtubules of graphitic carbon. Nature 354:56–58. doi:10.1038/354056a0

Kim B, Chung H, Kim W (2012) High-performance supercapacitors based on vertically aligned carbon nanotubes and nonaqueous electrolytes. Nanotechnology 23:155401. doi:10.1088/0957-4484/23/15/155401

Kukovecs A, Konya Z, Nagaraju N, Willems I, Tamasi A, Fonseca A, Nagy JB, Kiricsi I (2000) Catalytic synthesis of carbon nanotubes over Co, Fe and Ni containing conventional and sol-gel silica-aluminas. Phys Chem Chem Phys 2:3071–3076. doi:10.1039/B002331K

Kumar R, Singh RK, Ghosh AK, Sen R, Srivastava SK, Tiwari RS, Srivastava ON (2013) Synthesis of coal-derived single-walled carbon nanotube from coal by varying the ratio of Zr/Ni as bimetallic catalyst. J Nanopart Res 15:1406. doi:10.1007/s11051-012-1406-3

Lee CJ, Park J, Yu JA (2002) Catalyst effect on carbon nanotubes synthesized by thermal chemical vapor deposition. Chem Phys Lett 360:250–255. doi:10.1016/S0009-2614(02)00831-X

Lee SY, Yamada M, Miyake M (2005) Synthesis of carbon nanotubes over gold nanoparticle supported catalyst. Carbon 43:2654–2663. doi:10.1016/j.carbon.2005.05.045

Liu H, Zhang Y, Arato D, Li R, Mérel P, Sun X (2008) Aligned multi-walled carbon nanotubes on different substrates by floating catalyst chemical vapor deposition: critical effects of buffer layer. Surf Coat Technol 202:4114–4120. doi:10.1016/j.surfcoat.2008.02.025

Nessim GD, Hart AJ, Kim JS, Acquaviva D, Oh J, Morgan CD, Seita M, Leib JS, Thompson CV (2008) Tuning of vertically-aligned carbon nanotube diameter and areal density through catalyst pre-treatment. Nano Lett 8:3587–3593. doi:10.1021/nl801437c

Rakitin A, Papadopoulos C, Xu JM (2003) Carbon nanotube self-doping: calculation of the hole carrier concentration. Phys Rev B 67:033411. doi:10.1103/PhysRevB.67.033411

Reina A, Hofmann M, Zhu D, Kong J (2007) Growth mechanism of long and horizontally aligned carbon nanotubes by chemical vapor deposition. J Phys Chem C 111:7292–7297. doi:10.1021/jp0711500

Ryu H, Singh BK, Bartwal KS (2008) Synthesis and optimization of MWCNTs on Co-Ni/MgO by thermal CVD. Adv Cond Mat Phys. doi:10.1155/2008/971457

Sun LF, Mao JM, Pan ZW, Chang BH, Zhou WY, Wang G, Qian LX, Xie SS (1999) Growth of straight nanotubes with a cobalt-nickel catalyst by chemical vapor deposition. Appl Phys Lett 74:644–646. doi:10.1063/1.123027

Tawfick S, O'Brien K, Hart AJ (2009) Flexible high-conductivity carbon-nanotube interconnects made by rolling and printing. Small 5:2467–2473. doi:10.1002/smll.200900741

Teo KBK, Chhowalla M, Amaratunga GAJ, Milne WI, Hasko DG, Pirio G, Legagneux P, Wyczisk F, Pribat D (2001) Uniform patterned growth of carbon nanotubes without surface carbon. Appl Phys Lett 79:1534–1536. doi:10.1063/1.1400085

Wang Y, Luo Z, Li B, Ho PS, Yao Z, Shi L, Bryan EN, Nemanich RJ (2007) Comparison study of catalyst nanoparticle formation and carbon nanotube growth: support effect. J Appl Phys 101:124310. doi:10.1063/1.2749412

Yenilmez E, Wang Q, Cheng RJ, Wang D, Dai H (2002) Wafer scale production of carbon nanotube scanning probe tips for atomic force microscopy. Appl Phys Lett 80:2225–2227. doi:10.1063/1.1464227

Yin X, Wang Q, Lou C, Zhang X, Lei W (2008) Growth of multi-walled CNTs emitters on an oxygen-free copper substrate by chemical-vapor deposition. Appl Surf Sci 254:6633–6636. doi:10.1016/j.apsusc.2008.04.040

Zhang R, Xie H, Zhang Y, Zhang Q, Jin Y, Li P, Qian W, Wei F (2013) The reason for the low density of horizontally aligned ultralong carbon nanotube arrays. Carbon 52:232–238. doi:10.1016/j.carbon.2012.09.025

Zhao J, Zhang Y, Su Y, Huang X, Wei L, Kong ESW, Zhang Y (2012) Structural improvement of CVD multi-walled carbon nanotubes by a rapid annealing process. Diam Relat Mater 25:24–28. doi:10.1016/j.diamond.2012.01.029